UNCLASSIFIED

[redacted]

Copy 93

NASA MEMO 5-17-59A

NASA MEMO 5-17-59A

3

NASA

MEMORANDUM

THE EFFECT OF NOSE SHAPE ON THE STATIC AERODYNAMIC CHARACTERISTICS OF BALLISTIC-TYPE MISSILE MODELS AT MACH NUMBERS FROM 0.6 TO 1.4

By Stuart L. Treon

Ames Research Center
Moffett Field, Calif.

CLASSIFICATION CHANGED TO UNCLASSIFIED
BY AUTHORITY OF NASA CLASSIFICATION CHANGE
NOTICES, CHANGE NO. 214-45, EFF. 5/20/71
Jm

CLASSIFIED DOCUMENT - TITLE UNCLASSIFIED

This material contains information affecting the National Defense of the United States within the meaning of the espionage laws, Title 18, U.S.C., Secs. 793 and 794, the transmission or revelation of which in any manner to an unauthorized person is prohibited by law.

NATIONAL AERONAUTICS AND SPACE ADMINISTRATION

WASHINGTON

May 1959

[redacted]

UNCLASSIFIED

17966

NATIONAL AERONAUTICS AND SPACE ADMINISTRATION

MEMORANDUM 5-17-59A

THE EFFECT OF NOSE SHAPE ON THE STATIC AERODYNAMIC CHARACTERISTICS OF BALLISTIC-TYPE MISSILE MODELS AT MACH NUMBERS FROM 0.6 TO 1.4*

By Stuart L. Treon

SUMMARY

Results are presented for a wind-tunnel investigation of the effect of nose shape on the static aerodynamic characteristics of ballistic-type missile models at Mach numbers from 0.6 to 1.4 and angles of attack up to 14°. Reynolds number for the tests was 0.9 million referred to the model base diameter.

The effect of nose shape on the normal force and center-of-pressure location was small; axial force, however, was significantly affected both in variation with Mach number and in magnitude. A blunt-cylinder-nosed model had the greatest variations with Mach number of the measured aerodynamic characteristics as well as the highest values of axial-force coefficient. Above Mach number 1.1, use of spike-mounted flow deflectors resulted in reductions of axial force from that for the basic blunt-nosed model which were as large as 35 percent at a Mach number of 1.4. Use of certain flow deflectors, however, caused increases in the axial force at subsonic speeds.

A good approximation of the normal force and center of pressure of one of the test models was made by means of a combined application of potential and viscous crossflow theories.

INTRODUCTION

The selection of a suitable nose shape for a ballistic missile must necessarily take into account not only the re-entry heating problem but also the effect of the nose shape on the static and dynamic characteristics of the vehicle throughout the design Mach number range. Although

*Title, Unclassified

forces and moments of regular, pointed bodies of revolution have been estimated theoretically and measured experimentally at transonic speeds, there is relatively little information available for axisymmetric bodies having irregular or blunt noses.

The present investigation was conducted primarily to determine at transonic speeds the effects of nose shapes on the static aerodynamic characteristics of ballistic-type missile models. Included in the investigation was the measurement of the axial force of a blunt-nosed model equipped with disks or cones mounted on a spike in front of the nose. These flow deflectors were intended to reduce the drag by effectively increasing the fineness ratio of the nose.

NOTATION

C_A axial-force coefficient, $\frac{\text{axial force}}{qS}$

C_{A_o} axial-force coefficient at 0° angle of attack

C_m pitching-moment coefficient referred to the nose-body juncture, $\frac{\text{pitching moment}}{qSd}$

C_N normal-force coefficient, $\frac{\text{normal force}}{qS}$

$\frac{C_N}{\alpha}$ normal-force parameter; that is, the slope of the straight line drawn from the origin to any point on the C_N vs. α curve

d model base diameter

M free-stream Mach number

q free-stream dynamic pressure

S model base area

α angle of attack, deg

APPARATUS AND MODELS

The investigation was conducted in the Ames 2-foot transonic wind tunnel. This tunnel is described in reference 1; its principal feature is its ventilated test section which permits continuous choke-free operation to Mach number 1.4.

Five different configurations were investigated to determine the effects of nose shape. Each configuration (see fig. 1(a)) consisted of a cylindrical body having, for all five models, the same length and diameter to which were affixed the various noses. Pertinent dimensions of the noses are shown in the figure, and it is to be noted that all the noses were not of the same length. The fineness ratios of the complete configurations consequently varied from 5.25 to 5.92.

Model number 4 (see fig. 1(a)) was used to examine the effects of flow deflectors mounted forward of a blunt-nosed body. The arrangements tested are depicted in figure 1(b). As shown in this figure there were, in all, 24 variations of two basic flow deflector configurations tested - 19 of these being circular flat plates and 5 being right circular cones.

Pointed- and blunt-nosed models of various sizes were tested to determine the effect of wall interference which is discussed in the appendix. Sketches and dimensions of these models are presented in figure 1(c).

All models were sting-supported as shown in figure 2. Normal and axial forces, together with pitching-moment reactions, were measured by use of an internally mounted strain-gage balance similar to that described in reference 1.

The sizes and locations of the boundary-layer trip wires used in the various phases of the investigation are noted in figure 1.

TESTS AND DATA REDUCTION

Normal force, axial force, and pitching moment were measured for models 1 through 5 equipped with boundary-layer trip wires. The angle-of-attack range was -4° to 11° at Mach numbers of 0.6, 0.8, 0.9, 1.0, 1.1, 1.2, and 1.4. Additional axial-force data for these models were obtained at 0° angle of attack at intermediate Mach numbers considered sufficient to define the variations of axial force with Mach number. Data were also obtained for models 3 and 5 without trip wires at conditions corresponding to those for the models with trip wires. Model 4 with flow deflectors was tested without trip wires to obtain axial-force data at 0° angle of attack at Mach numbers of 0.6, 0.8, 0.9, 1.0, 1.1, 1.2, 1.3, and 1.4.

The boundary-layer condition of the models, without and with trip wires, was investigated briefly by means of subliming compounds in a manner suggested by references 2 and 3. Observations were made at Mach numbers of 0.8 and 1.2 at angles of attack of 0° and 8°. In order to distinguish between regions of laminar and separated boundary layers (for which the subliming solid residue on the model might appear to be similar), an established procedure was followed of placing small projections on the surface of the model. The projections produced wedge-shaped patterns of turbulence in the subliming material if the flow on the model was basically laminar, but had no apparent effect in regions of separated flow.

The basic Reynolds number for the force and moment tests was 0.9 million referred to the model base diameter. For models 2 and 5, however, the Reynolds number was decreased approximately 10 percent at $M = 1.4$ because of a power limitation of the main drive motors.

Force and moment coefficients are referred to the body axes and are based on the area and diameter of the model base. The moment reference point is located on the model axis of symmetry at the nose-body juncture which for all models is 3.79 body diameters forward of the model base.

Corrections have been applied to the model angles of attack for deflection of the model support and balance resulting from aerodynamic loads, and to the axial forces to make them equivalent to what would have been obtained had the base pressure been equal to free-stream static pressure.

Subsonic wall interference corrections to the data were estimated by the method of reference 4 and were found to be negligibly small. The wall interference at sonic speed was estimated according to equations of reference 5. This latter estimate suggested extremely large corrections to the Mach number for the data of the blunt-nosed models. In order to establish the applicability of the method of reference 5 to blunt shapes, and to provide an experimental indication of wall interference for the models of this report, a separate investigation of wall interference was made, the results of which are discussed in the appendix. These results indicate that no significantly large or systematic wall interference on the data of the nose shape investigation exists. Corrections for air-stream angularity and test-section Mach number gradient are unnecessary, as may be seen from inspection of the data contained in reference 1.

Apart from the possible small systematic errors caused by wall interference, the data are considered to be correct within the following maximum random errors of measurement, as evaluated by the method of reference 6:

M	± 0.003
α	$\pm .02^{\circ}$
C_A	$\pm .002$
C_m	$\pm .02$
C_N	$\pm .02$

RESULTS AND DISCUSSION

Effect of Nose Shape

Representative basic data are presented in figure 3 for three of the seven test Mach numbers. These data pertain to models 1 through 5 with boundary-layer trip wires and also to models 3 and 5 without trip wires. More detailed indications of the effects of nose shape on the longitudinal characteristics of the models with trip wires are provided in figures 4, 5, and 6; these are variations with Mach number of normal-force parameter, center of pressure, and axial-force coefficient at 0° angle of attack, respectively. The effect of trip wires on the axial force is summarized in figure 7 for models 3 and 5. The foregoing results are discussed in subsequent sections along with the theoretical results described next.

Theoretical variations of normal-force and pitching-moment coefficients with angle of attack are presented in figure 3(a) for model 1; theoretical values of the normal-force parameter and center of pressure for model 1 as a function of Mach number are shown in figures 4 and 5, respectively. In making the theoretical calculations for model 1, it was assumed that the model could be treated as though it had a conical nose. The theoretical method followed was that of reference 7 in which viscous crossflow theory and potential theory are combined. The potential theory was that of reference 8 for subsonic speeds and reference 9 for sonic and supersonic speeds. For the supersonic case, reference 9 includes consideration of the potential normal force resulting from aerodynamic interference between the conical nose and the cylindrical body; for the present application, the simplifying assumption was made that the center of this interference normal force was at the cone-cylinder juncture, which was also the moment reference station. It was further assumed that the potential normal force of the nose was at the centroid of the cone plan area. In calculating the viscous cross forces on the model, it was also assumed that these cross forces did not occur on the conical nose because of the likelihood of favorable pressure gradients acting to prevent flow separation.

The boundary-layer flow patterns on the models defined by the subliming solid technique were recorded both in sketches and in photographs. Because of the lack of sufficient clarity, however, the photographs were not suitable for reproduction herein. It was possible, though, to obtain a good indication of the boundary-layer flow characteristics from careful examination of the sketches and photographs. The flow characteristics are discussed in the following section of the report. This information will aid in the understanding of the results of the force and moment tests to be discussed later.

Boundary-layer flow characteristics.- For the models without trip wires at 0° angle of attack, only model 3 (which had a pointed nose) had any significant laminar boundary-layer run. The transition from laminar to turbulent flow at $M = 0.8$ took place at about 50 percent of the model 3 nose length; at $M = 1.2$, transition occurred at about 75 percent of the nose length (rearward from the tip). The other models had separated flow over the forward parts of the noses - the flow being turbulent upon reattachment. For models 1, 2, and 4, the flow separation extended downstream from immediately behind the nose tips approximately 10 percent of the respective nose lengths at the test conditions investigated. For the model with the cylindrical nose (model 5), the extent of the flow separation varied greatly with Mach number at 0° angle of attack as shown in figure 8. Separated flow extended the length of the cylindrical nose at $M = 0.8$ and about 30 percent of the cylindrical nose length at $M = 1.2$.

At 8° angle of attack, the only marked change in the boundary-layer flow patterns from those observed for the various models at 0° angle of attack was observed for model 5 (fig. 8). For this model at $M = 0.8$, the extent of flow separation at 8° angle of attack was about one-third as great as that which existed at 0° angle of attack.[1]

Placement of 0.004-inch-diameter trip wires on the model noses at the locations shown in figure 1(a) had a noticeable effect on the boundary-layer flow of model 3 only. The boundary-layer transition moved forward to the wire location on model 3, whereas there were no changes in the flow patterns on the other models.

[1]Some results of tests subsequent to this investigation indicate the possibility that the data presented herein for model 5 do not completely define its longitudinal characteristics. These later results for a model similar to the nose of model 5 indicate, at sonic speeds and above, differing longitudinal characteristics for increasing and decreasing angles of attack. The data for the present report were obtained only for increasing angles.

Normal-force characteristics.- The effect of nose shape on the normal-force characteristics was surprisingly small considering the wide range of nose shapes investigated (figs. 3 and 4). Furthermore, there was but little effect of Mach number on the normal-force parameter.

For model 1 theory and experiment agreed within about 15 percent at 0° angle of attack and within about 10 percent at higher angles of attack - good first approximations. Because of the small effect of nose shape, there was similar agreement between the theoretical estimates for model 1 and the experimental results for the other models.

Center of pressure.- As in the case of the normal force, the effects of nose shape and Mach number on the center-of-pressure location were, in general, small (fig. 5). Model 5, however, had a more rearward location of the center of pressure as well as a more extensive over-all center-of-pressure variation with Mach number at 0° angle of attack than did the other models. Such characteristics are considered to be related to the flow separation patterns previously described for the nose of this model.

The theoretical estimate of the center-of-pressure location for model 1 agreed within less than one-half body diameter with the model 1 experimental results - again, a good first approximation. It follows that there would be similar agreement between the model 1 estimate and the test results for models 2, 3, and 4, and poorer agreement with the model 5 results.

Axial force at 0° angle of attack.- As might be expected with large changes in nose shape, there were significant differences in axial-force coefficient among the various models both in variation with Mach number and in magnitude (fig. 6). However, not all of the differences might have been anticipated from a simple examination of the model nose shapes. There were, for example, for models 1 and 2, which had the same nose radius and fineness ratio, generally large differences in coefficient values, particularly at transonic speeds (calculations according to slender body theory suggested only slightly lower values for model 2 because it had a smaller mean cone angle, as determined taking into account the angle and base area of each cone segment). Also, there was less difference between the results for blunted model 2 and pointed model 3 than the difference in bluntness suggested but for which a possible explanation is provided in reference 10. Furthermore, only model 4 had an increasing value of axial-force coefficient at 0° angle of attack throughout the Mach number range. On the other hand, model 5, despite its higher fineness ratio, had values of axial-force coefficient considerably higher than those for model 4.

The effect of trip wires on the axial-force data of models 3 and 5 is presented in figure 7. Based upon the previously discussed boundary-layer flow patterns observed at $M = 1.2$, a difference in axial-force coefficient was expected for model 3 as tested with and without a trip wire. The experimental difference was in good agreement with an estimate made using skin-friction-coefficient values of reference 11 and taking into account the noted differences in extent of turbulent boundary layer (the experimental difference in the coefficients for the model without and with a trip wire was 0.011 compared with an estimated value of 0.008). For $M = 0.8$ the trip wire had little effect on the drag which was in accord with the fact that the turbulent boundary-layer run was the same with or without a trip wire on the model. The apparent inconsistency of the data for model 5 at $M = 1.15$ (shown by the two-level data points) was the result of the appearance and disappearance of an oblique shock wave on the model nose as observed by means of schlieren apparatus. The wave appeared when the separated flow on the forward part of the model nose reattached; when this occurred, the axial-force coefficient increased for model 5 both without and with trip wires.

Effect of Flow Deflectors

The complete results of the tests of the effect of flow deflectors on axial force for the basic blunt-nosed model 4 are presented in table I. Representative plots of the data for two of the more favorable deflector arrangements, from the standpoint of axial-force reduction at supersonic speeds, are presented in figure 9 for comparison with data for the basic model. Use of either the cone or disk deflector effected a reduction of axial-force coefficient from that for the reference model which began at about $M = 1.1$ and amounted to as much as 35 percent at $M = 1.4$. A generally smaller reduction of axial force at supersonic speeds resulted from use of any of the test flow deflectors. Although the cone-deflector configuration showed an increase in axial-force coefficient amounting to approximately 10 percent at $M = 1.0$, it showed little or no increase at lower Mach numbers. For the disk-deflector configuration, however, there was an increase in axial force over that for the reference model of as much as 46 percent at subsonic speeds (increases for other disk-deflector configurations ranged from about 4 percent to as much as 72 percent). It is to be noted that the variations of axial force with Mach number for model 4 with the more effective flow deflectors were similar to those for the more slender-nosed models 2 and 3, and were considerably different from those for model 4 alone.

CONCLUDING REMARKS

An experimental investigation has been made to determine the effect of nose shape on the static aerodynamic characteristics of a ballistic-type missile model at Mach numbers from 0.6 to 1.4. The following remarks are based upon the results of this program.

1. In general, nose shape had a small effect on both the normal force and the location of the center of pressure; the axial force, however, was significantly affected both in variation with Mach number and in magnitude.

2. Good approximations of the experimental normal-force and center-of-pressure results for one of the test models were made by means of a combined application of potential and viscous crossflow theories.

3. The model with the blunt-cylinder nose had the greatest variations with Mach number of the measured aerodynamic characteristics, and also had the highest values of axial-force coefficient.

4. Use of either a cone or disk flow deflector ahead of the bluntest model tested reduced axial-force coefficient at Mach numbers above 1.1. Use of certain flow deflectors on the blunt-nosed model resulted in variations of axial force with Mach number similar to those for more slender-nosed models.

Ames Research Center
National Aeronautics and Space Administration
Moffett Field, Calif., Feb. 17, 1959

APPENDIX

INTERFERENCE OF POROUS WALL TEST SECTIONS

Wall interference in porous wall test sections for Mach numbers near 1 may be attributed to two factors: (a) shock-wave reflections from the walls impinging upon the model, and (b) pressure reflections associated with blockage. The first of these two types ordinarily results in an erratic but negligible fluctuation of the force coefficients of models with cylindrical afterbodies between, roughly, 1.0 to 1.15 Mach number. Relatively little information is available regarding the effect of the second.

One method of estimating the magnitude of the second type of interference is suggested in the appendix of reference 5. According to this method, in its most simplified form, the interference at sonic speed is treated as a Mach number error and can be calculated by the equations

$$\Delta M = -0.82 \left(\frac{r^*}{h}\right)^{6/7} \left(\frac{r^*}{x^*}\right)^{2/7}$$

$$M_\infty = 1 - \Delta M$$

where M_∞ is the indicated Mach number in the wind tunnel, h is the half-tunnel height, and x^* and r^* are the coordinates of the sonic point on the body surface (measured rearward from the tip and perpendicular to the longitudinal axis, respectively).

An examination of the equation for ΔM suggests for blunt shapes, on which the sonic point would likely be far forward, that large corrections to the tunnel Mach number would be required even for models small relative to the cross section of the test section. To test the validity of this hypothesis and provide a means for appraising the interference existing in the current tests, force data were measured for three different sizes of two models which were chosen to represent sharp-nosed and blunt-nosed configurations. These models, referred to hereafter as "model A" and "model B," correspond closely to models 3 and 5, respectively; outline drawings and dimensions pertaining to them are presented in figure 1(c). Ratios of the parameter (r^*/h) were 0.023, 0.041, and 0.059 for model A, and 0.012, 0.021, and 0.030 for model B. The largest values of (r^*/h) for models A and B, respectively, were the same as those for corresponding models 3 and 5. The sonic point was assumed to be at the base of the first nose cone section for model A and at the edge of the front cylinder face for model B. Model A was tested with trip wires and model B with none. The tests were made at 0° angle of attack at Mach numbers from 0.6 to 1.2. The Reynolds number was 0.49 million referred to the model base diameter.

Results of the tests are presented in figure 10 as plots of axial-force coefficient versus Mach number for all three sizes of both model A and model B. Three things are immediately apparent from inspection of this figure. First, there are neither significantly large nor systematic differences in the data suggestive of wall interference at $M = 1.0$, a result quite in contrast to that expected from the theoretical analysis, particularly in the case of model B. Second, there were differences of a somewhat systematic nature in the data for model A at approximately $M = 1.04$ for which there is no ready explanation but which are considered relatively unimportant. Third, the erratic variations observable in the results for the largest model of configuration A between $M = 1.05$ and 1.13 are typical of models upon which wave reflections have impinged (according to schlieren observations, reflected waves impinged on the models of the nose shape investigation up to $M = 1.2$, and hence there would be the possibility of such interference up to that Mach number).

On the basis of these results, therefore, it may be said that there was no significantly large or systematic wall interference on the data for the sizes of models tested.

REFERENCES

1. Spiegel, Joseph M., and Lawrence, Leslie F.: A Description of the Ames 2- by 2-Foot Transonic Wind Tunnel and Preliminary Evaluation of Wall Interference. NACA RM A55I21, 1955.

2. Main-Smith, J. D.: Chemical Solids as Diffusible Coating Films for Visual Indications of Boundary-Layer Transition in Air and Water. British R.&M. No. 2755, 1950.

3. Winter, K. G., Scott-Wilson, J. B., and Davies, F. V.: Methods of Determination and of Fixing Boundary-Layer Transition on Wind Tunnel Models at Supersonic Speeds. British MOS A.R.C. C.P. No. 212, Sept. 1954. (Also ARC Rep. 17,416, R.A.E. TN Aero. 2341, and AGARD Rep. AG17/P7)

4. Baldwin, Barrett S., Jr., Turner, John B., and Knechtel, Earl D.: Wall Interference in Wind Tunnels with Slotted and Porous Boundaries at Subsonic Speeds. NACA TN 3176, 1954. (Supersedes NACA RM A53E29)

5. Page, William A.: Experimental Study of the Equivalence of Transonic Flow About Slender Cone-Cylinders of Circular and Elliptic Cross Section. NACA TN 4233, 1958.

6. Beers, Yardley: Introduction to the Theory of Error. Addison-Wesley Publishing Company, Inc., Cambridge, Mass., 1953.

7. Allen, H. Julian, and Perkins, Edward W.: A Study of Effects of Viscosity on Flow Over Slender Inclined Bodies of Revolution. NACA Rep. 1048, 1951. (Supersedes NACA TN 2044)

8. Munk, Max M.: The Aerodynamic Forces on Airship Hulls. NACA Rep. 184, 1924.

9. Moskowitz, Barry: Approximate Theory for the Calculation of Lift of Bodies, Afterbodies, and Combinations of Bodies. NACA TN 2669, 1952.

10. Hart, Roger G.: Flight Investigation at Mach Numbers from 0.8 to 1.5 to Determine the Effects of Nose Bluntness on the Total Drag of Two Fin-Stabilized Bodies of Revolution. NACA TN 3549, 1955. (Supersedes NACA RM L50I08a)

11. Locke, F. W. S., Jr.: Recommended Definition of Turbulent Friction in Incompressible Fluids. NAVAER DR Rep. No. 1415, June 1952.

TABLE I.- VALUES OF AXIAL-FORCE COEFFICIENT AT 0° ANGLE OF ATTACK FOR MODEL 4 AND VARIOUS FLOW DEFLECTOR CONFIGURATIONS

C_{A_o} for model 4 plus cone flow deflector

M \ l, in.	3/4	1-1/8	1-1/2	1-7/8	2-1/4
0.6	0.075	0.084	0.096	0.091	0.083
.8	.081	.085	.097	.100	.092
.9	.112	.118	.126	.130	.126
1.0	.170	.175	.184	.187	.189
1.1	.235	.239	.244	.243	.238
1.2	.260	.253	.246	.236	.228
1.3	.277	.260	.247	.224	.216
1.4	.289	--	.242	--	.212

C_{A_o} for model 4 plus disk flow deflector, d_1 = 3/8 in.

M \ l, in.	3/4	1-1/8	1-1/2	1-7/8	2-1/4
0.6	0.077	0.091	0.106	0.121	0.126
.8	.077	.090	.102	.116	.129
.9	.108	.117	.127	.137	.145
1.0	.165	.176	.182	.188	.198
1.1	.229	.238	.236	.232	.234
1.2	.248	.240	.233	.228	.227
1.3	.262	.239	.232	.227	.224
1.4	.271	--	.230	.224	.221

C_{A_o} for model 4 plus disk flow deflector, d_1 = 1/4 in.

M \ l, in.	3/4	1-1/8	1-1/2	1-7/8	2-1/4
0.6	0.078	0.087	0.099	0.097	0.089
.8	.081	.086	.099	.106	.103
.9	.113	.118	.125	.131	.136
1.0	.170	.176	.182	.187	.195
1.1	.235	.239	.245	.241	.241
1.2	.258	.251	.245	.236	.232
1.3	.279	.260	.244	.232	.225
1.4	.295	--	.241	--	.219

C_{A_o} for model 4 plus disk flow deflector, d_1 = 1/2 in.

M \ l, in.	3/4	1-1/8	1-1/2	1-7/8	2-1/4
0.6	0.082	0.099	0.114	0.131	0.149
.8	.081	.093	.108	.124	.141
.9	.111	.117	.128	.140	.154
1.0	.167	.175	.182	.190	.201
1.1	.236	.229	.227	.232	.241
1.2	.242	.232	.230	.231	.235
1.3	.250	.234	.232	.232	.235
1.4	.259	.237	.234	.233	.233

C_{A_o} for model 4 plus disk deflector, d_1 = 5/8 in.

M \ l, in.	3/8	3/4	1-1/8	1-1/2
0.6	0.072	0.082	0.101	0.126
.8	.073	.083	.096	.116
.9	.108	.108	.120	.135
1.0	.163	.165	.173	.187
1.1	.227	.228	.226	.234
1.2	.251	.236	.234	.239
1.3	.272	.243	.240	.244
1.4	.292	.252	--	.249

M	C_{A_o} for model 4
0.6	0.086
.8	.092
.9	.117
1.0	.172
1.1	.249
1.2	.278
1.3	.311
1.4	.341

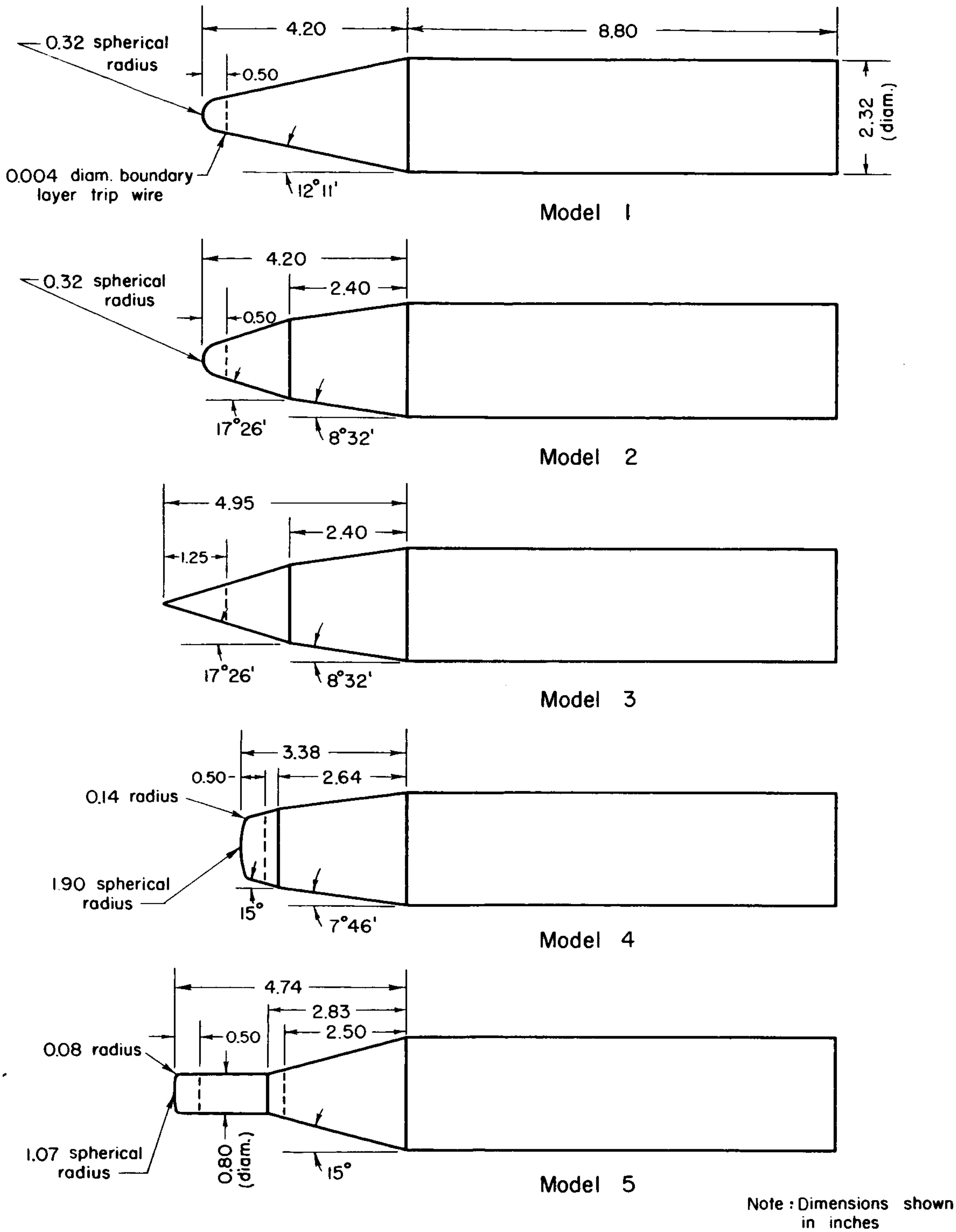

(a) Nose-afterbody models.

Figure 1.- Model sketches and dimensions.

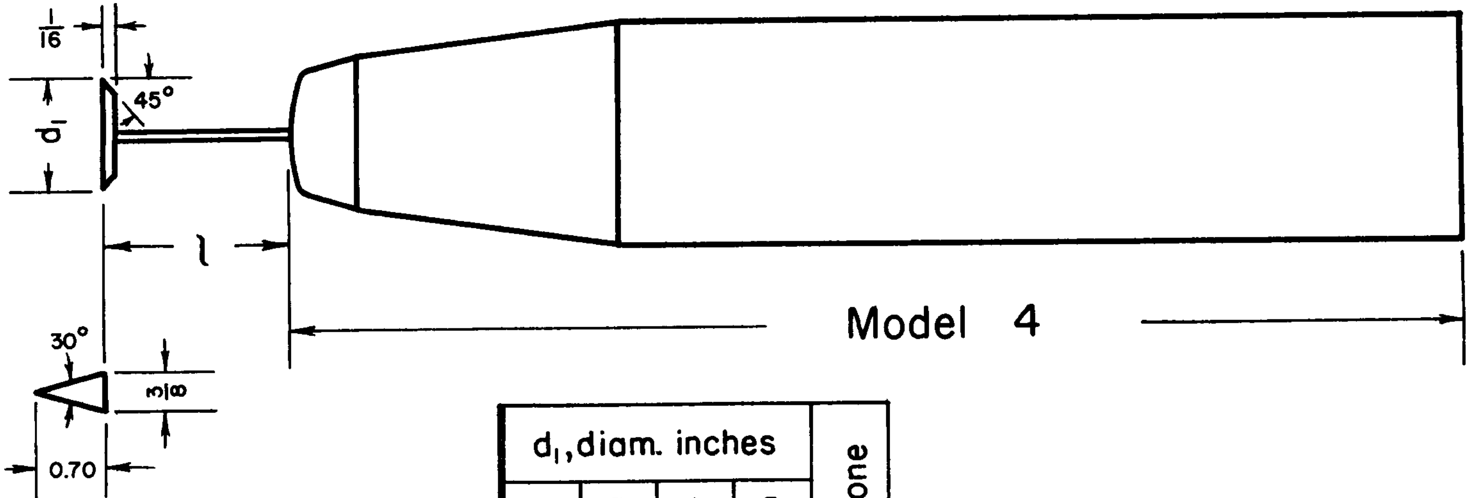

Note : Dimensions shown in inches

		d_1, diam. inches				Cone
		$\frac{1}{4}$	$\frac{3}{8}$	$\frac{1}{2}$	$\frac{5}{8}$	
l, inches	$\frac{3}{8}$				X	
	$\frac{3}{4}$	X	X	X	X	X
	$1\frac{1}{8}$	X	X	X	X	X
	$1\frac{1}{2}$	X	X	X	X	X
	$1\frac{7}{8}$	X	X	X		X
	$2\frac{1}{4}$	X	X	X		X

Note: "x" denotes model tested

(b) Flow deflector models.

Figure 1.- Continued.

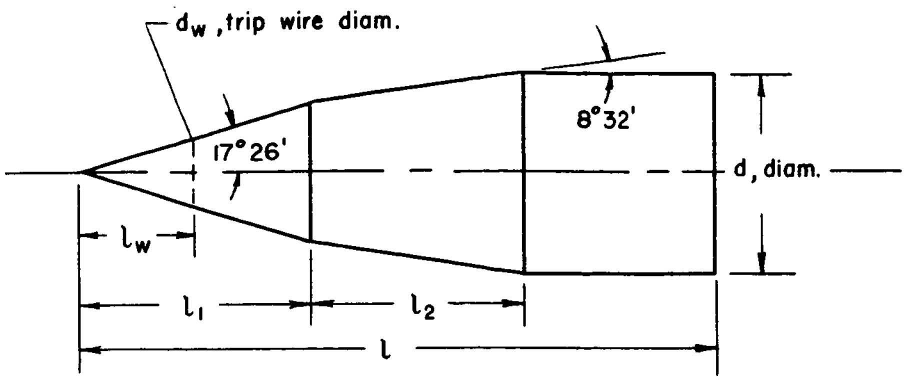

Model	r^*/h	l_1	l_2	l	d	l_w	d_w
A	0.023	1.00	0.94	2.85	0.91	0.50	0.004
	0.041	1.76	1.66	5.02	1.60	0.88	0.005
	0.059	2.55	2.40	7.27	2.32	1.28	0.007

Note: 1) Dimensions shown in inches

2) r^*/h defined in appendix

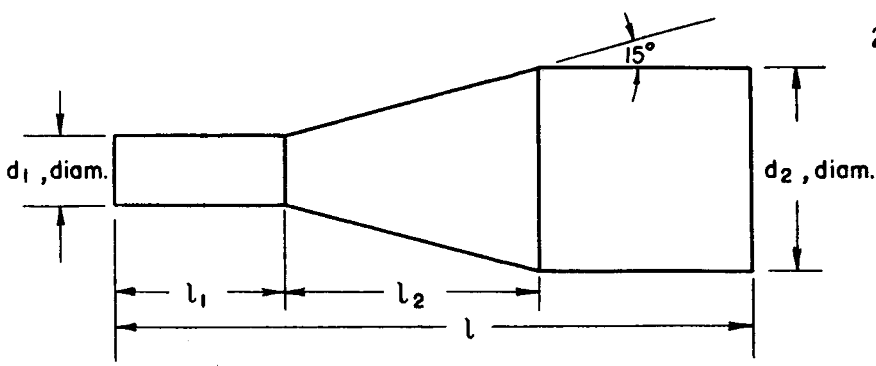

Model	r^*/h	l_1	l_2	l	d_1	d_2
B	0.012	0.76	1.14	2.82	0.32	0.92
	0.021	1.32	1.97	4.89	0.56	1.60
	0.030	1.91	2.85	7.08	0.80	2.32

(c) Interference investigation models.

Figure 1.- Concluded.

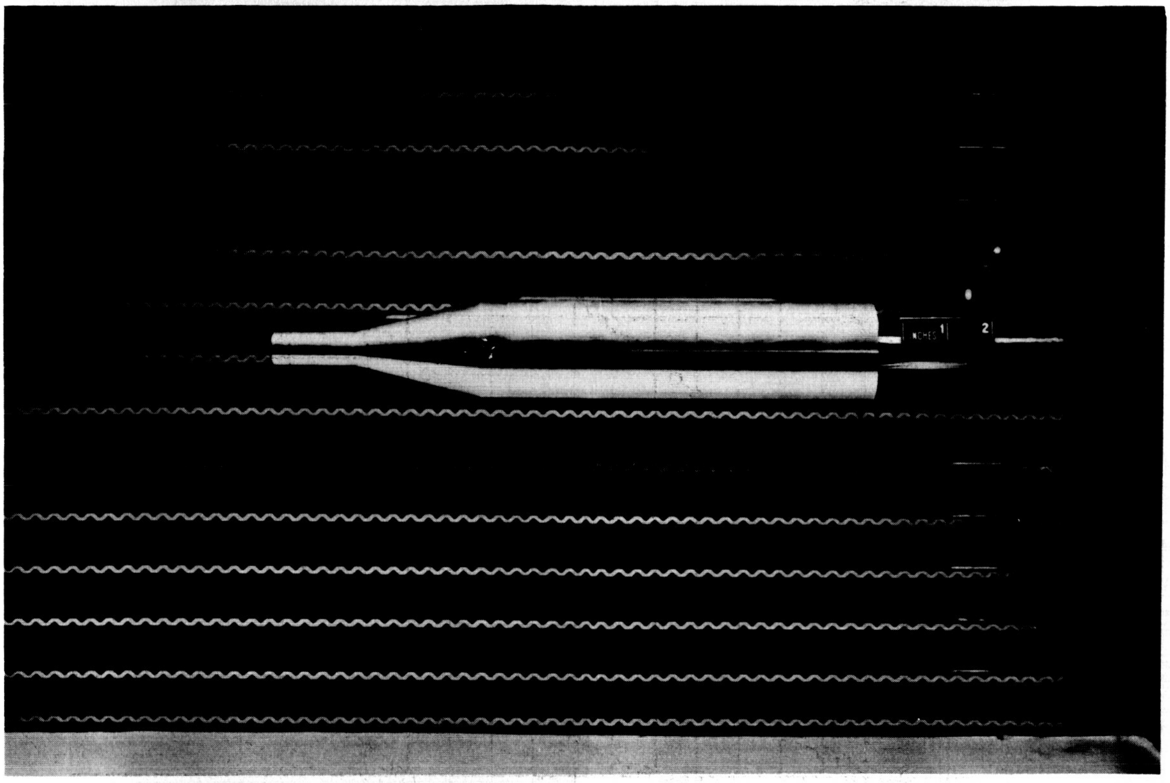

A-22826

Figure 2.- Representative model installed in the Ames 2- by 2-foot transonic wind tunnel test section.

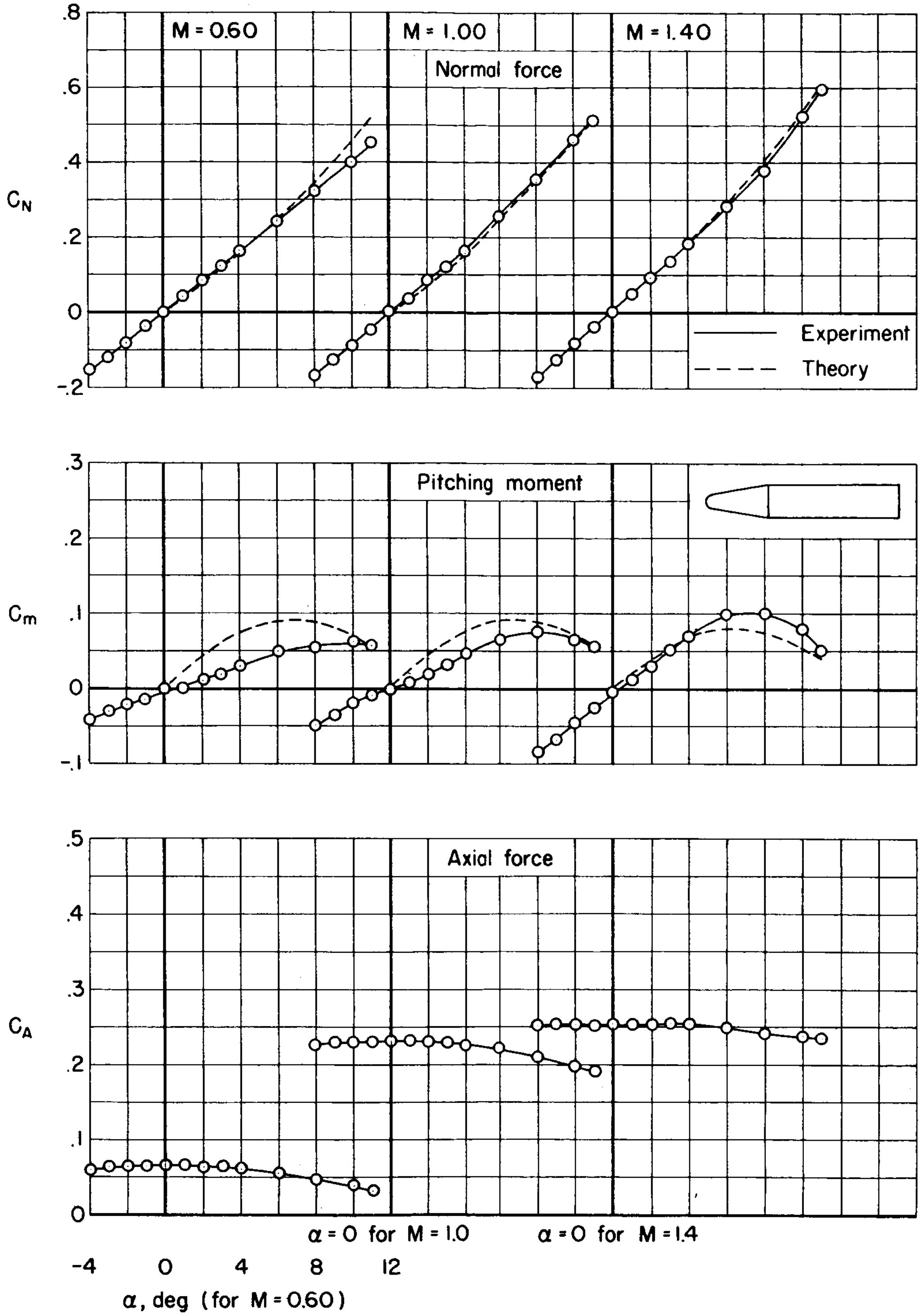

(a) Model 1, with trip wire.

Figure 3.- Representative static longitudinal characteristics.

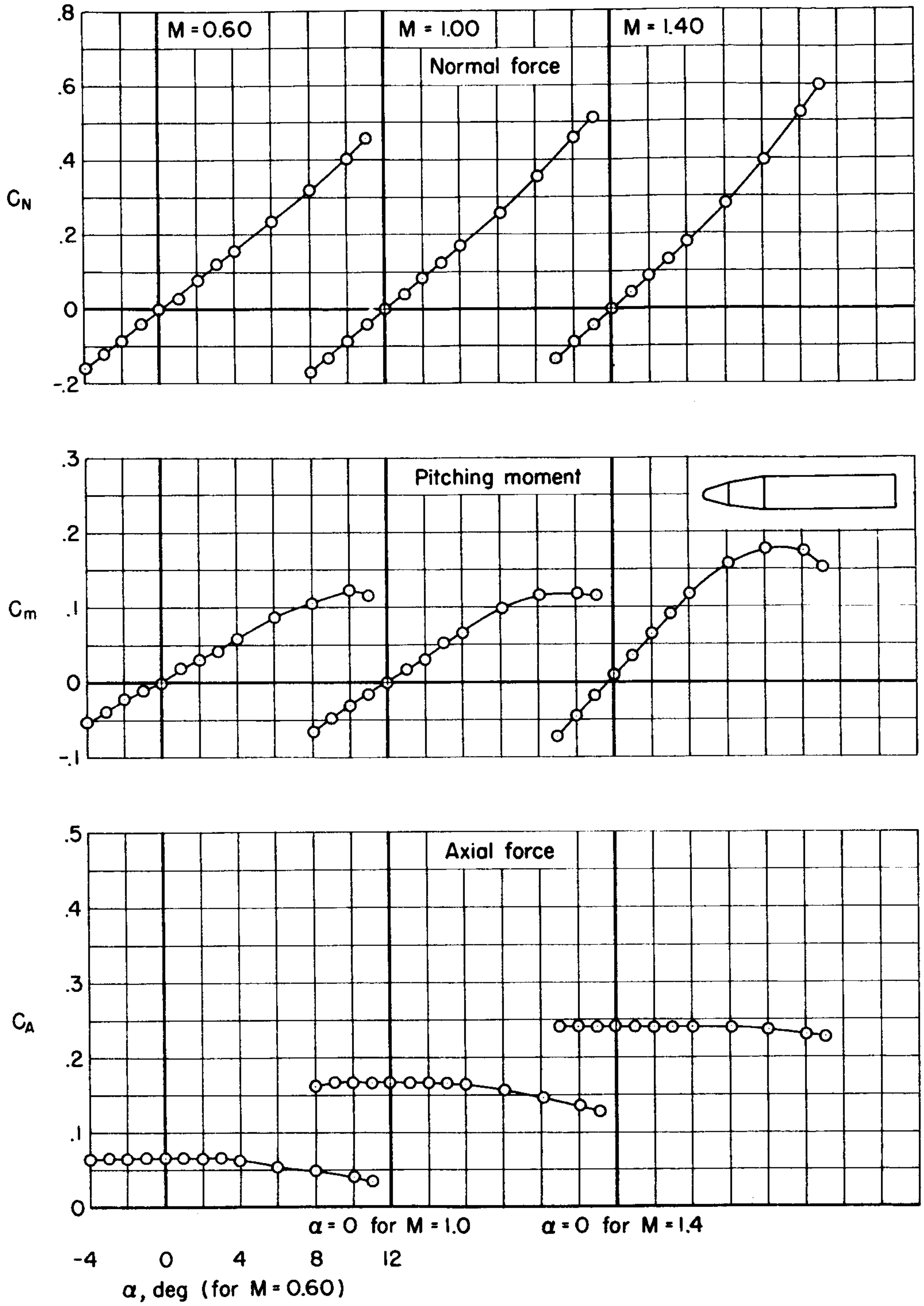

(b) Model 2, with trip wire.

Figure 3.- Continued.

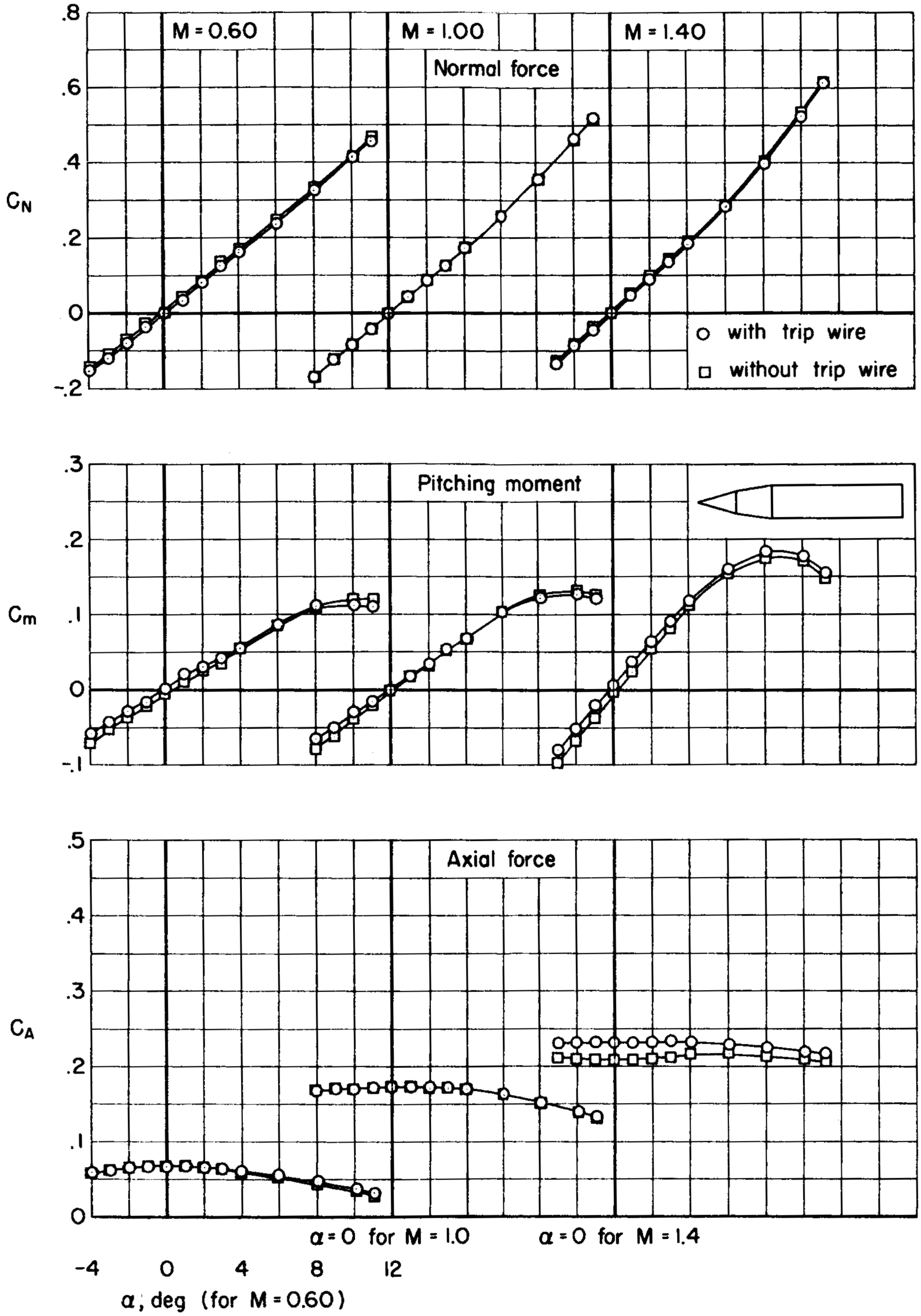

(c) Model 3, with and without trip wire.

Figure 3.- Continued.

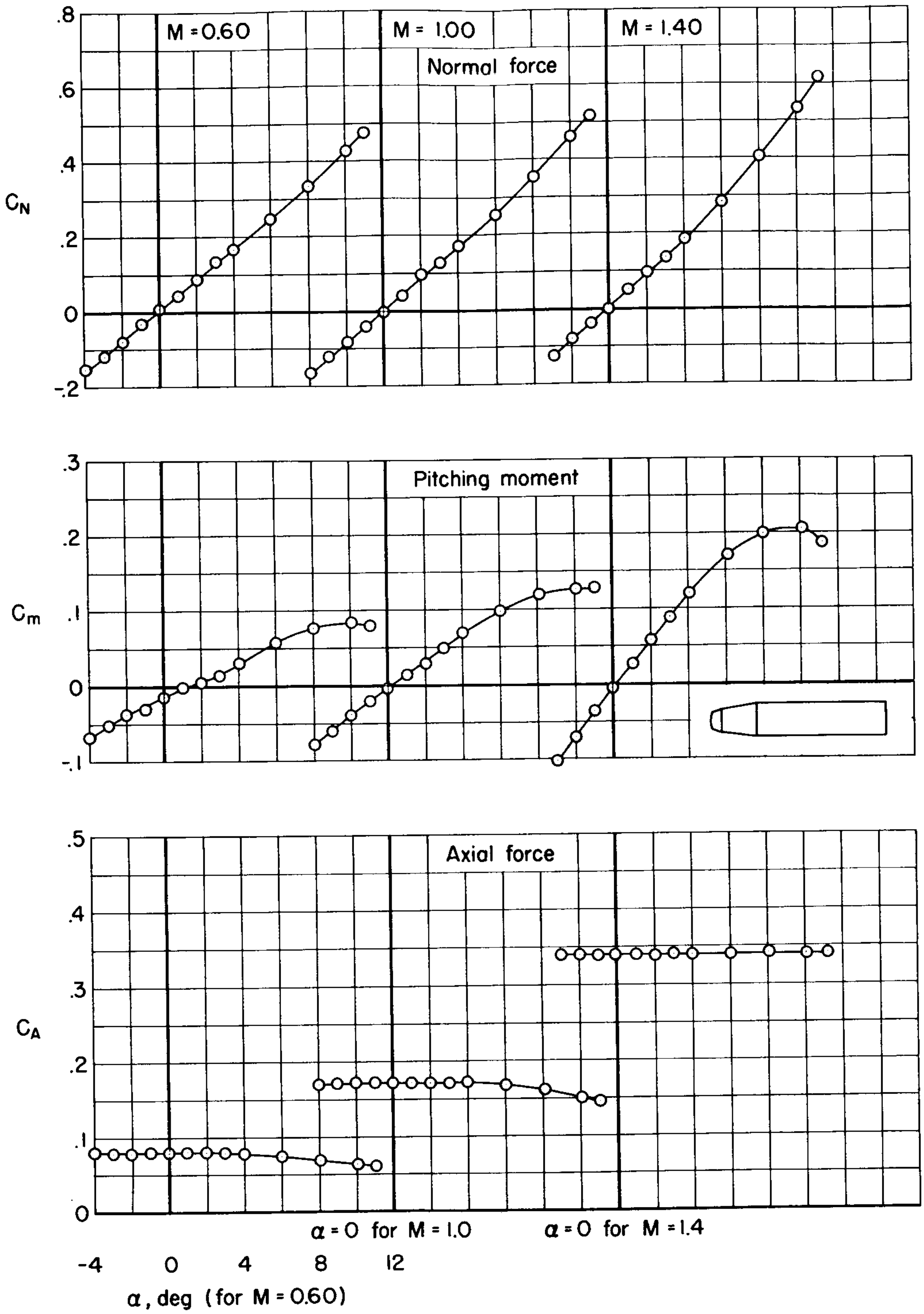

(d) Model 4, with trip wire.

Figure 3.- Continued.

[redacted]

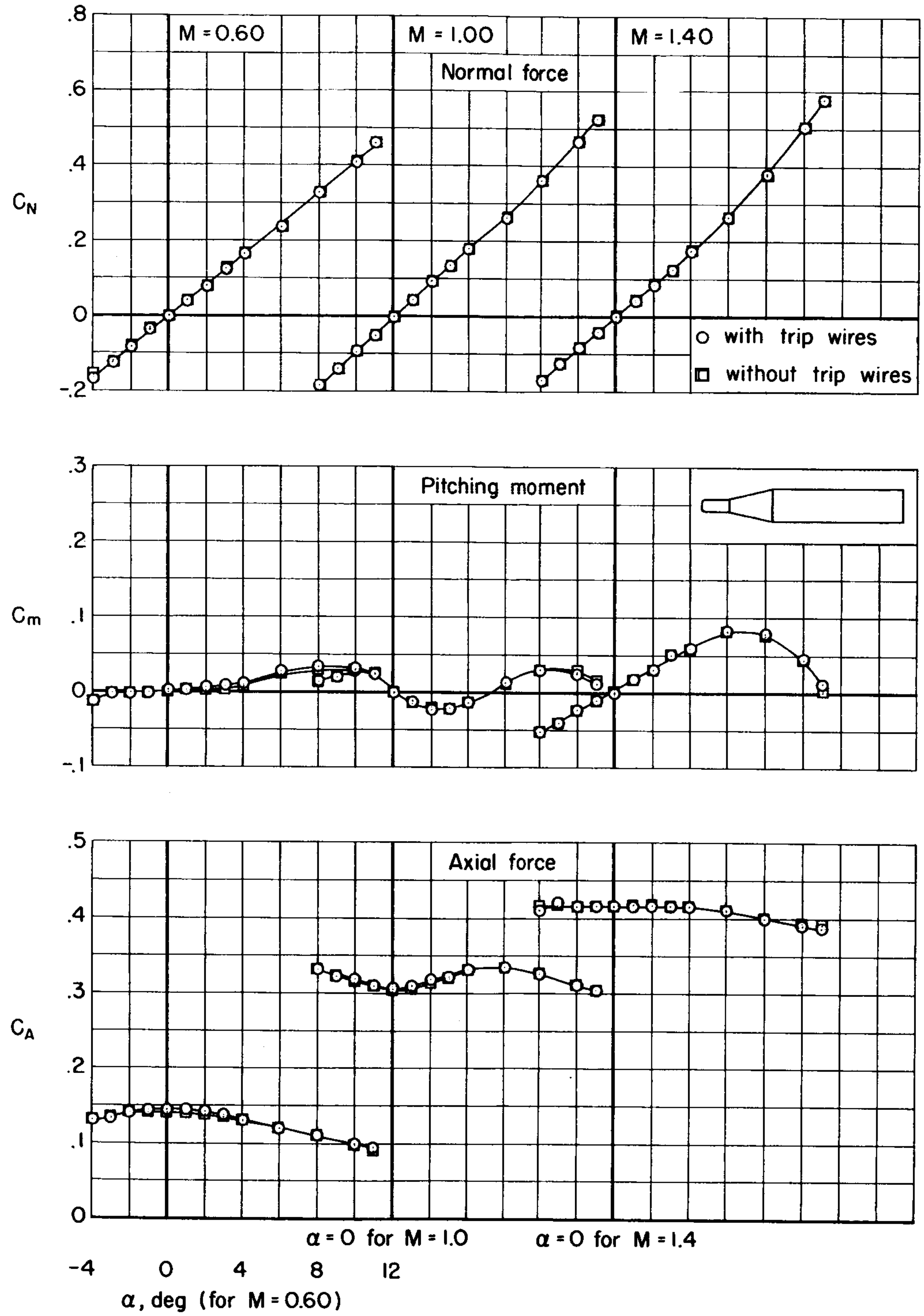

(e) Model 5, with and without trip wires.

Figure 3.- Concluded.

[redacted]

[redacted]

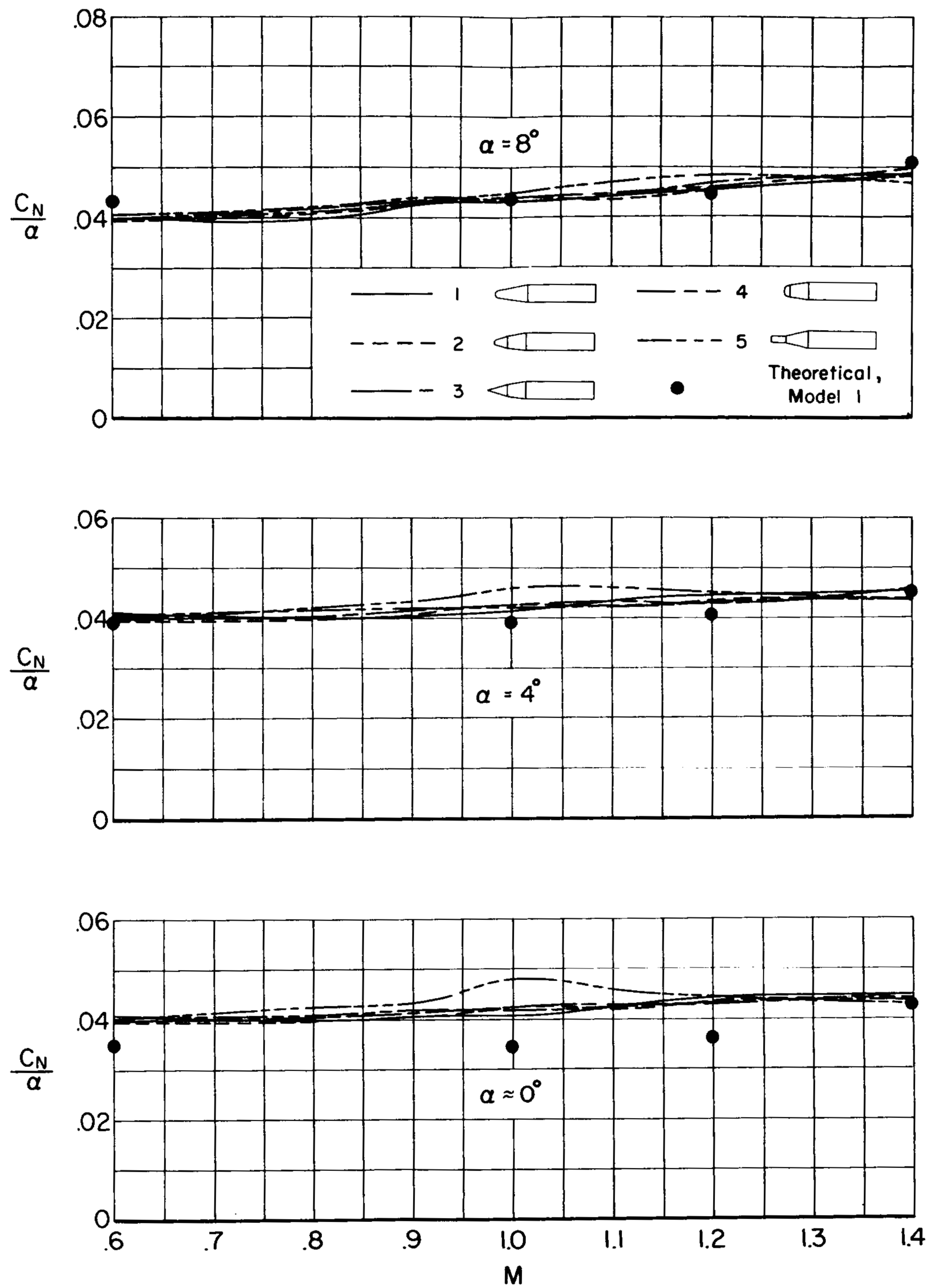

Figure 4.- Effect of nose shape on the variation of normal-force parameter with Mach number for the models equipped with boundary-layer trip wires.

[redacted]

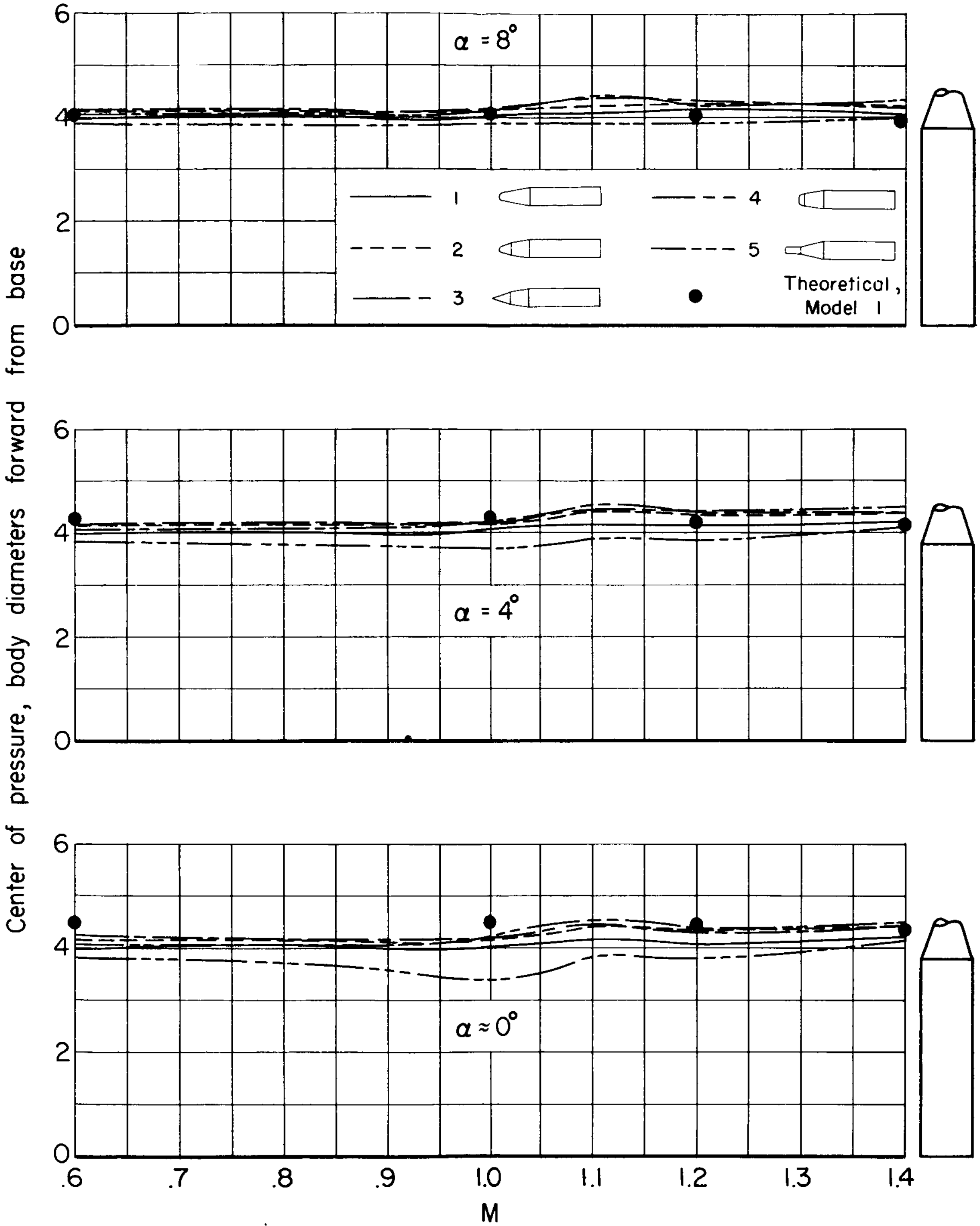

Figure 5.- The effect of nose shape on the variation of the center of pressure with Mach number for the models equipped with boundary-layer trip wires.

[redacted]

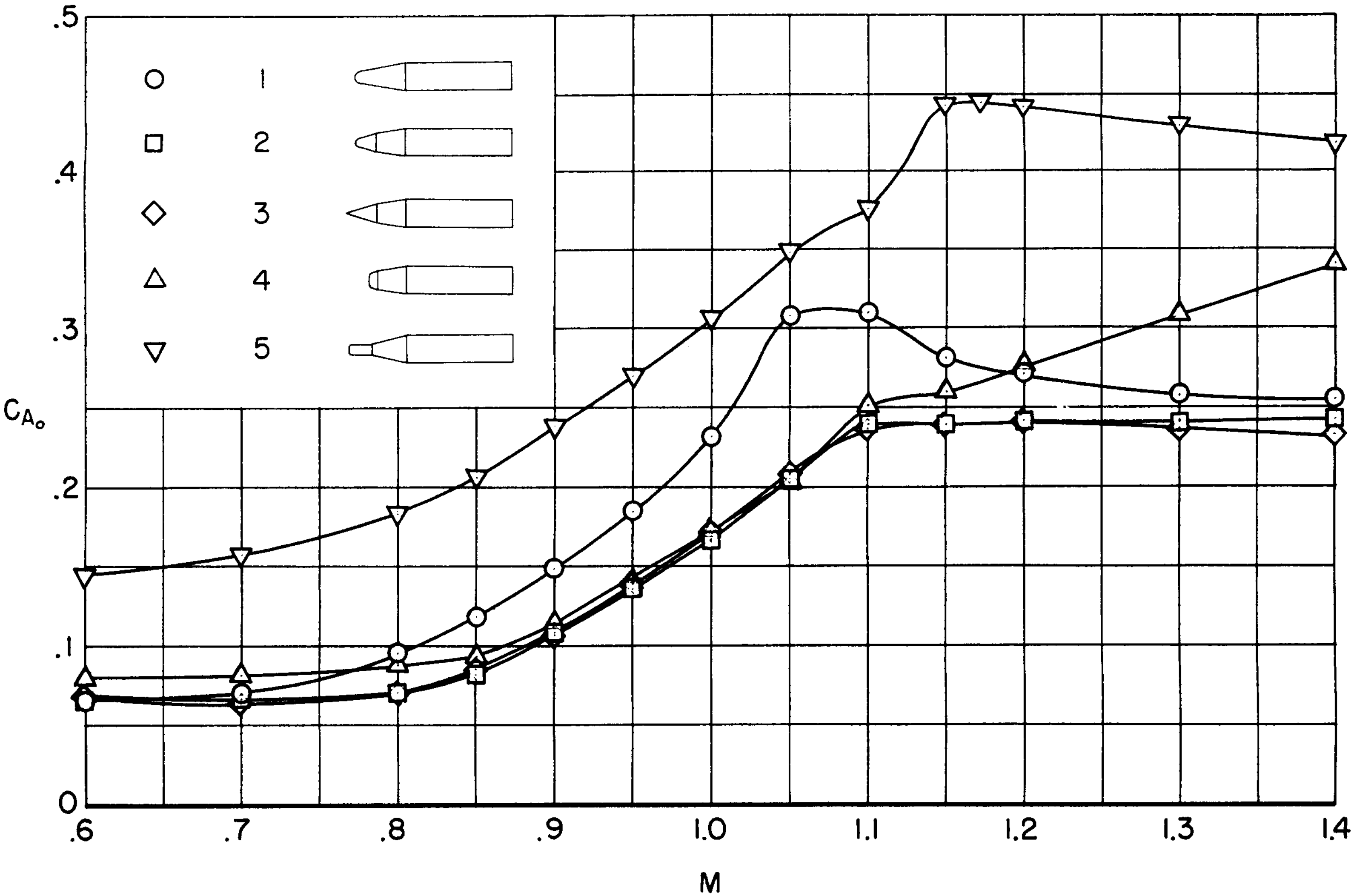

Figure 6.- Effect of nose shape on the variation with Mach number of axial-force coefficient at 0° angle of attack for the models equipped with boundary-layer trip wires.

CONF[redacted]AL

[redacted]

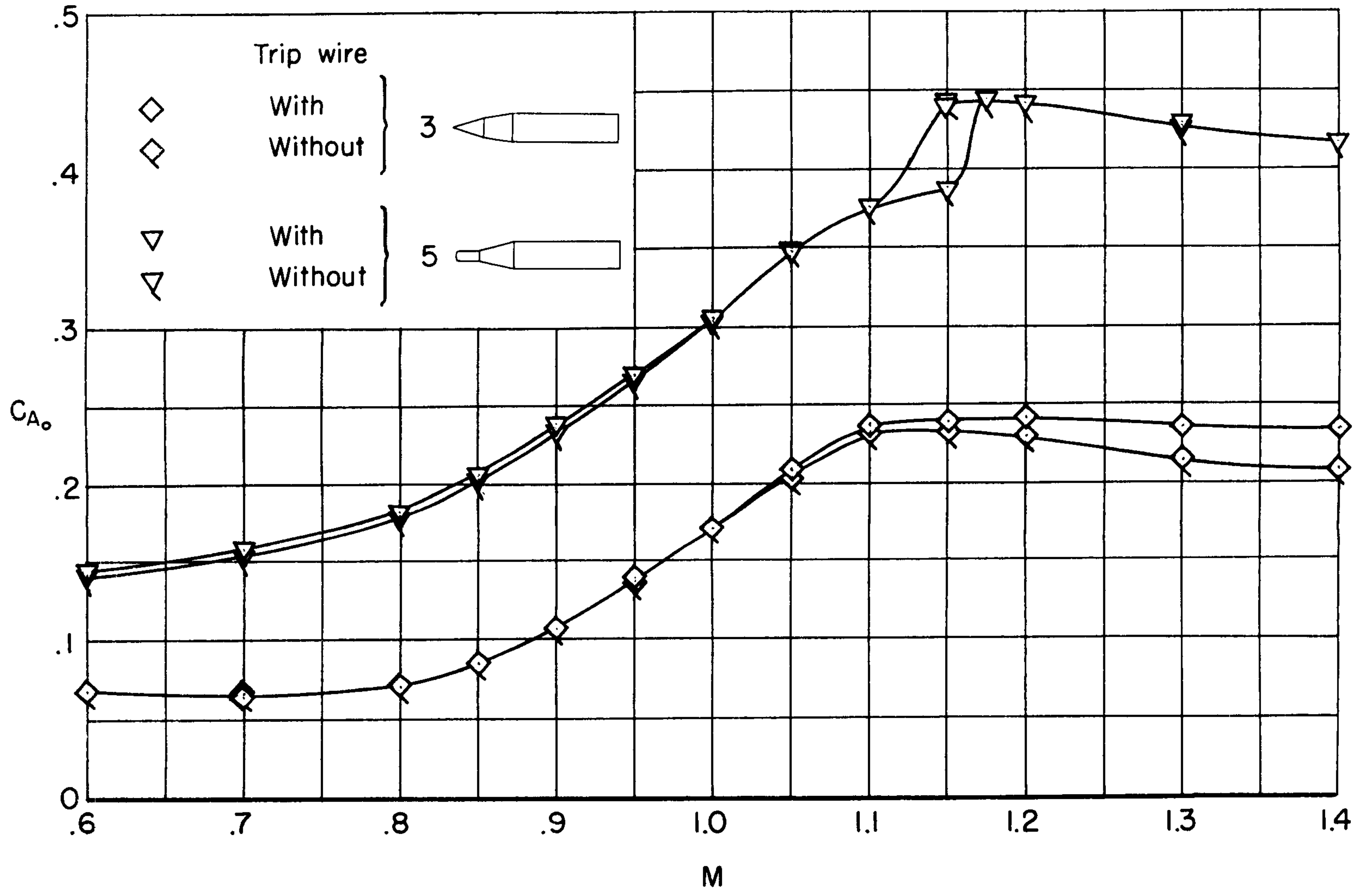

Figure 7.- Effect of boundary-layer trip wires on the variation with Mach number of axial-force coefficient at 0° angle of attack for two models.

[redacted]

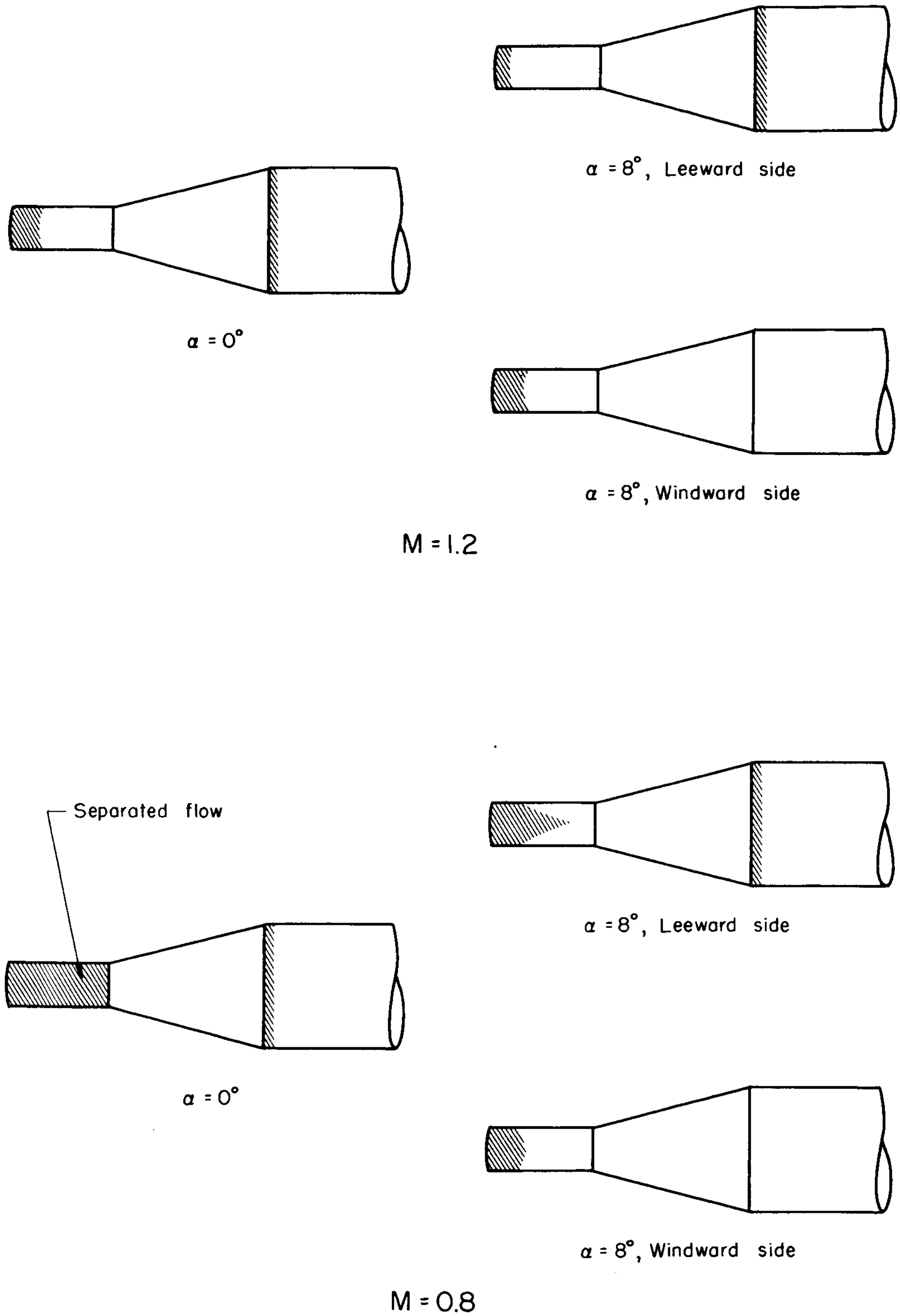

Figure 8.- Sketches of separated flow patterns for model 5.

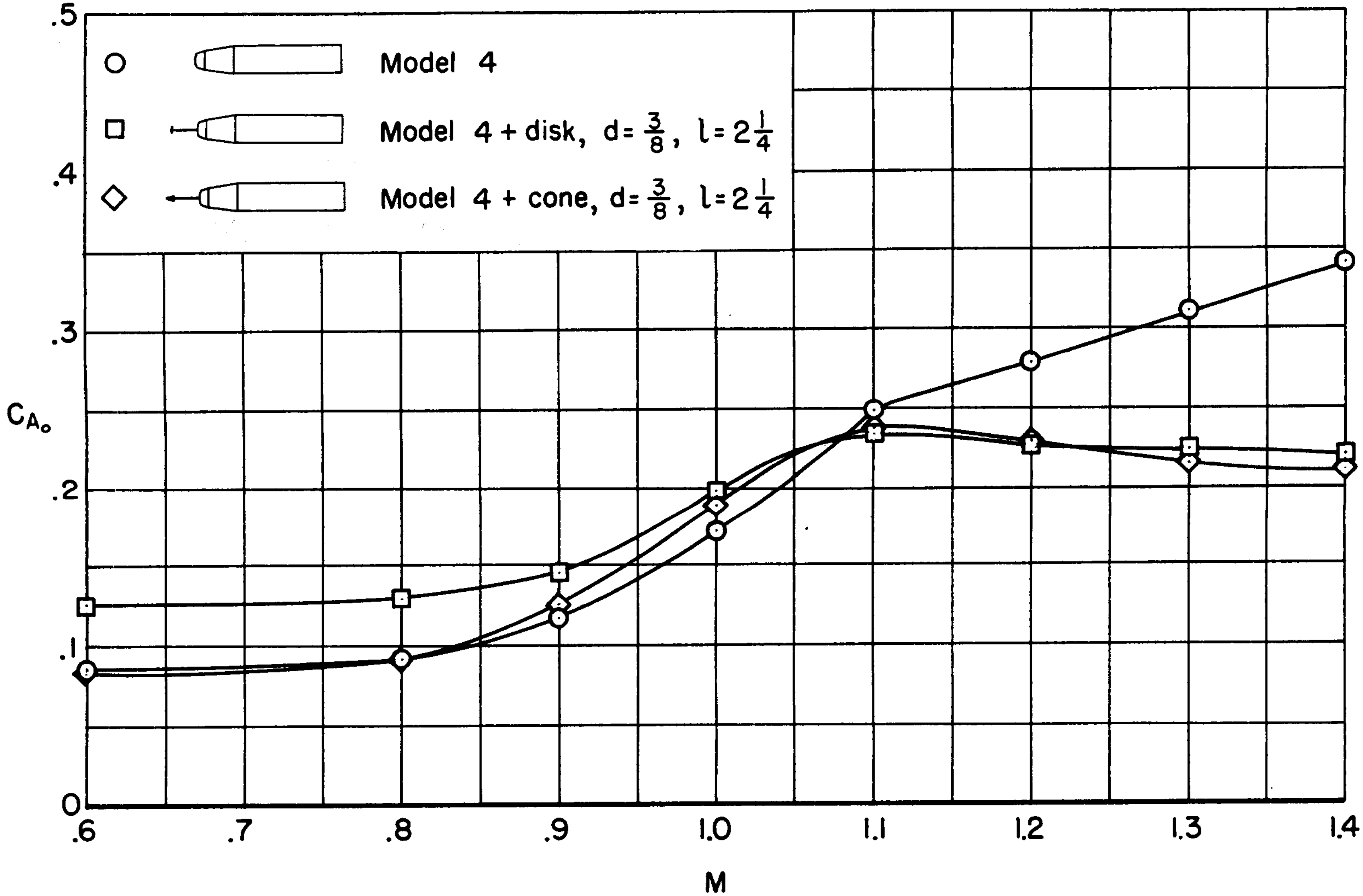

Figure 9.- Variation with Mach number of axial-force coefficient at 0° angle of attack for model 4 alone and with two flow deflector configurations.

[redacted]

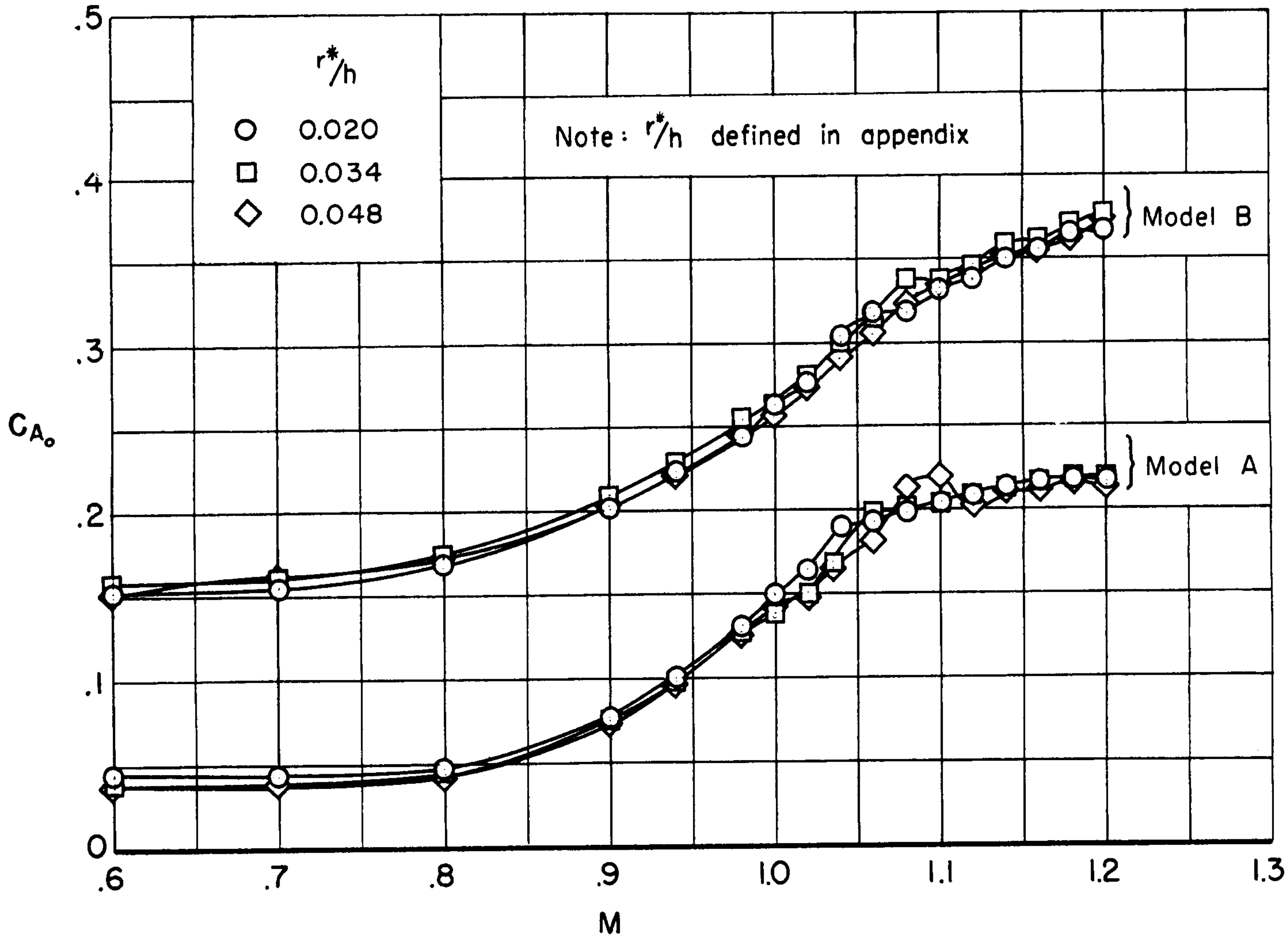

Figure 10.- The effect of model size on the variation with Mach number of axial-force coefficient at 0° angle of attack.

[redacted]